Adaptive Repetitive Control of DFIG-DC System Considering Stator Frequency Variation

Chao Wu, Heng Nian, *Senior Member, IEEE*, Bo Pang, and Peng Cheng

***Abstract*—This paper presents an adaptive repetitive control method for torque ripple suppression of the doubly fed induction generator (DFIG) system connected to a dc grid considering the stator frequency variation. Since the stator of DFIG is connected to the the diode bridge directly, the stator frequency should be controlled additionally. A novel frequency-locked loop (FLL) based on a second-order generalized integrator (SOGI) is proposed for acquiring stator frequency. The stator fundamental voltage is obtained by the adaptive multi-SOGI. Thus, the low-pass filter can be avoided, which can improve the bandwidth of the control loop. Furthermore, the orientation angle can be acquired by the stator fundamental voltage vector directly, which can avoid the parameter dependence on stator and rotor inductances. Since the stator frequency will be controlled to change in a certain range for efficiency optimization, an adaptive repetitive controller (RC) is added to the rotor current control loop for torque ripple suppression considering the stator frequency variation. Based on a mathematical model of the DFIG control system, the transfer function of the frequency control loop and the torque control loop are derived for analyzing the control performance and parameter design. Finally, the proposed control method is validated through the experiment results.**

***Index Terms*—Doubly fed induction generator (DFIG), frequency-locked loop (FLL), second-order generalized integrator (SOGI), torque ripple suppression.**

I. Introduction

UP TO now, wind energy utilization has become one of the most predominant renewable power generation. Due to the advantages such as flexible regulation of active and reactive power and lower requirement for converter capacity, the doubly fed induction generator (DFIG) has been broadly applied for wind turbine [1], [2]. In order to implement the stable operation and effective energy conversion of the DFIG-based wind turbine, there are two alternative grid connection topology options for wind farms connecting to the grid, namely, alternating current (ac) and direct current (dc) grid connection. The ac grid connection is always used for the on-shore wind farm. Due to the long distance and large capacity of power transmission, the high-voltage direct current (HVDC) connection is a superior way for the offshore wind farm [3]. Thus, it is significant for investigating the DFIG-DC topology and the corresponding control strategy.

Manuscript received March 18, 2018; revised May 10, 2018 and June 19, 2018; accepted July 2, 2018. Date of publication July 8, 2018; date of current version February 20, 2019. This work was supported by the National Science Foundation of China under Grant 51622706. Recommended for publication by Associate Editor A. J. M. Cardoso. *(Corresponding author: Heng Nian.)*

C. Wu, H. Nian, and B. Pang are with the College of Electrical Engineering, Zhejiang University, Hangzhou 310027, China (e-mail:

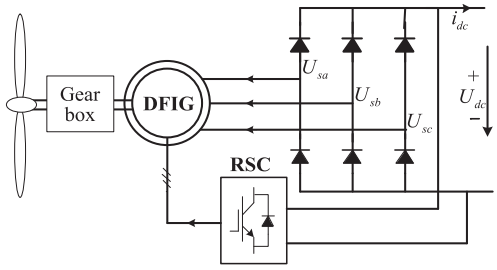

Fig. 1. DFIG connected to a dc link through a diode rectifier.

Currently, a DFIG-DC topology, as shown in Fig. 1, has been widely studied. In this topology, the DFIG is connected to the dc grid just by one converter on the rotor side and one diode bridge on the stator side. In this way, the cost is reduced and the configuration is simper compared with the traditional ac-grid-connected DFIG system for the dc transmission [4]–[6]. However, due to the stator-side diode bridge, the control strategy applied in the ac grid mode is not suitable in this DFIG-DC topology.

There are several researches devoting in studying control strategies of the DFIG-DC topology [7]–[17]. Marques and Iacchetti have done some work in studying this topology [7]–[13]. First, the basic operation and design issues on the DFIG-DC system were initially studied in [7], which presented a decoupling control method to regulate the average torque and stator frequency. In [8] and [9], the stator voltage is used to calculate the angle of the stator flux linkage for the orientation in the control strategy, which is based on the integration of stator electromotive force (EMF). In [10] and [11], the sensorless operation of the DFIG-DC system is investigated to avoid the rotor position sensor. The stator voltage is applied in the phase-locked loop (PLL) for estimating the stator frequency. Since the stator voltage is highly distorted, a low-pass filter is used to reduce the frequency ripple, which will reduce the dynamic response of the frequency estimation block. In [12], a field-weakening method is proposed for the efficiency optimization of the DFIG-DC system, in which the stator frequency variation over a wide range should be ensured. Considering that the stator voltage is highly distorted, a resonant controller or a repetitive controller

(RC) was added in the control loop to suppress the torque ripple [13]–[15]. However, the existed resonant control or repetitive control for torque ripple only aimed at the fixed stator frequency and the stator frequency variation is not considered. In [16], a predictive delay compensation method is proposed for minimization of torque ripple, which copes with the stator frequency variation. However, the torque ripple minimization ability depends on the accuracy of advance time. In [17], a predictive torque and rotor flux control method is proposed to mitigate the torque ripple. Torque ripple can be effectively mitigated at a constant and variable stator frequency since the predictive control can be thought as an infinite bandwidth control. However, the performance of this method is highly dependent on the DFIG parameters.

In order to reduce the joule losses of the DFIG system and increase the wind power transmission efficiency, the stator flux amplitude of DFIG should be adjusted to decrease the copper losses of the rotor according to the output power level. Since the product of the stator flux amplitude and the stator frequency is constant, the stator frequency should be controlled to be variable according to the output power change for system efficiency optimization [12]. Furthermore, the torque ripple will deteriorate the fatigue strength and decrease the life time of mechanical components, which is also needed to be suppressed. Therefore, the problems for the DFIG-DC system in the existed literature can be concluded as follows:

1) The parameter dependence is high when estimating the stator frequency or achieving the stator flux orientation.
2) The stator frequency variation is not considered when designing the resonant controller or RC for torque ripple suppression.
3) The stator voltage or stator flux PLL is slow in acquiring the stator frequency which will deteriorate the adaptive repetitive control performance.

In order to achieve an adaptive RC when the stator frequency varies, the stator frequency is set as an input of the RC. Thus, the stator frequency should be observed quickly and smoothly. In this paper, for improving the dynamic performance of acquiring the stator frequency and reducing the stator frequency ripple, a novel stator frequency estimation method is proposed based on SOGI-FLL [18], [19]. For suppressing the torque ripple even with various stator frequency, an adaptive RC is applied in the control loop by accurately handling the fractional order delay [20]–[22]. In conclusion, based on the existed control strategy in the DFIG-DC system, there are three improvements that can be achieved in this paper.

1) The stator voltage PLL is substituted by the stator fundamental voltage FLL, which not only improves the dynamic performance of frequency estimation but also reduces the steady-state frequency ripple.
2) The orientation angle is directly obtained by the stator fundamental voltage vector, which avoids the parameter dependency on the stator and rotor inductance.
3) The efficiency optimization is achieved by weakening the stator flux, which corresponds to the increase of the stator frequency. An adaptive RC is presented for suppressing the torque ripple considering the increase of the stator frequency.

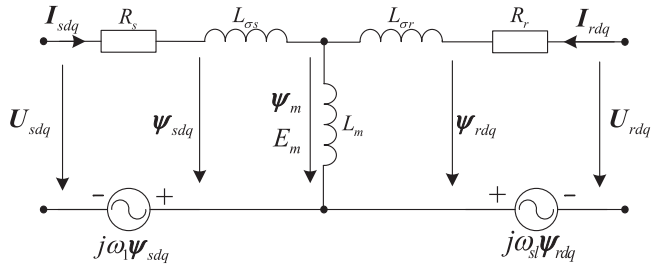

Fig. 2. DFIG equivalent circuit on the *d–q* reference frame.

This paper is organized as follows. The system layout and the mathematical model are outlined in Section II. The control strategy of RSC is elaborated in detail in Section III. Furthermore, the performance analysis of the proposed control strategy is presented in Section IV. Section V shows the experimental results, and the conclusion is made in Section VI.

II. System Layout and Mathematical Model

A. System Layout

The DFIG connected to the dc link is shown in Fig. 1, in which the stator and the rotor are connected to the dc link through a diode rectifier and a pulsewidth-modulated (PWM) converter, respectively. Differently from the conventional DFIG system with the ac grid connection, the grid-side converter is avoided. Considering dc voltage is usually stable in dc grid, the voltage of the dc link is assumed to be constant in this paper.

When the diode rectifier operates on the continuous operation mode, the stator voltage is clamped to the three-step square wave [13]. The stator phase voltage can be expressed as

$$U_{sa}(t) = \frac{2U_{dc}}{\pi}\left(\sin\omega_1 t + \sum_{n=1}^{\infty}\left(\frac{\sin(6n-1)\omega_1 t}{6n-1} + \frac{\sin(6n+1)\omega_1 t}{6n+1}\right)\right) \quad (1)$$

where $U_{\rm dc}$ is the dc voltage and ω_1 is the stator angular frequency.

As seen in (1), the fundamental voltage of the stator is fixed if the dc voltage is constant. It can be described as the product of stator frequency and stator flux, which can also be used for the regulation of the stator frequency and the orientation of stator flux [8], [9].

B. Mathematical Model

As can be seen in Fig. 1, the stator voltage is highly distorted due to the diode rectifier on the stator. Thus, the traditional voltage-oriented control (VOC) strategy based on PLL is not suitable for this topology. To achieve the vector control of DFIG in this topology, the stator flux orientation is adopted in this paper. The equivalent circuit of DFIG in the synchronized *d–q* reference frame is shown in Fig. 2, and the reference direction of the voltage and current is shown in Fig. 1.

According to Fig. 2, the stator and rotor voltages and flux linkage in the *dq* reference frame rotating at the synchronous

angular speed can be expressed as

$$\begin{cases} \boldsymbol{U}_s = R_s \boldsymbol{I}_s + \frac{d\boldsymbol{\psi}_s}{dt} + j\omega_1 \boldsymbol{\psi}_s \\ \boldsymbol{U}_r = R_r \boldsymbol{I}_r + \frac{d\boldsymbol{\psi}_r}{dt} + j\omega_{sl} \boldsymbol{\psi}_r \end{cases} \tag{2}$$

$$\begin{cases} \boldsymbol{\psi}_{sdq} = L_s \boldsymbol{I}_{sdq} + L_m \boldsymbol{I}_{rdq} \\ \boldsymbol{\psi}_{rdq} = L_m \boldsymbol{I}_{sdq} + L_r \boldsymbol{I}_{rdq} \end{cases} \tag{3}$$

where $\boldsymbol{U}$ is the voltage; ψ is the flux; $\boldsymbol{I}$ is the current; R_s and R_r are the stator and rotor resistances, respectively; ω_1 is the synchronous speed, which is equal to the stator angular frequency; ω_r is the rotor angular speed; and $\omega_{sl} = \omega_1 - \omega_r$ is the slip angular speed; $L_s = L_m + L_{\sigma s}$ and $L_r = L_m + L_{\sigma r}$ are the self-inductances of the stator and rotor windings; $L_{\sigma s}$, $L_{\sigma r}$, and L_m are the stator and the rotor leakage inductances and the mutual inductance, respectively; subscripts *s*, *r* represent the stator and the rotor, respectively; subscripts d and q represent the components at the *d–q* axis, respectively.

If the inverter losses are assumed to be proportional to the rotor current, which can be expressed as $P_{inv0} I_r$, the total joule losses P_J of the DFIG-DC system is given as

$$P_J = R_s I_s^2 + R_r I_{rd}^2 + R_r I_{rq}^2 + P_{\text{inv0}} I_r. \tag{4}$$

As can be seen from (4), when the output power of DFIG system is low, reducing the magnetization current will reduce the joule losses and improve the system efficiency. Since the detailed model of the DFIG-DC system efficiency optimization have been demonstrated in [12], it is not repeated in this paper. In conclusion, the field-weakening control should be applied at low output power for efficiency optimization and the corresponding result is the stator frequency variation. Thus, the stator frequency is controlled to be variable according to output power for reducing system losses.

Since the voltage drop on the stator resistance is very small in DFIG, the stator flux linkage can be expressed by the integrator of the stator voltage. Thus, based on the stator voltage expression (1), the stator flux vector in the *dq* reference frame can be expressed as

$$\boldsymbol{\psi}_{sdq} = \frac{2U_{dc}}{\pi\omega_1} \left(1 + \sum_{n=1}^{\infty} \frac{e^{j(\pm 6n\omega_1 t)}}{(1 \pm 6n)^2} \right). \tag{5}$$

Since the stator voltage is highly distorted in DFIG-DC system, the stator current and the rotor current are also distorted if no corresponding control solutions are adopted. Thus, the stator current can also be expressed by sum of fundamental components and harmonics as

$$\boldsymbol{I}_{sdq} = \boldsymbol{I}_{sdq1} + \sum_{n=1}^{\infty} \left(\boldsymbol{I}_{sdq(6n-1)} e^{-j6n\omega_1 t} + \boldsymbol{I}_{sdq(6n+1)} e^{j6n\omega_1 t} \right). \tag{6}$$

The torque can be represented by the stator flux linkage and stator current as

$$T_e = \text{Re}\left(j\boldsymbol{\psi}_{sdq} \hat{\boldsymbol{I}}_{sdq} \right) = \text{Re}\left(jL_m \boldsymbol{I}_{rdq} \hat{\boldsymbol{I}}_{sdq} \right) = T_{e0} + \sum_{n=1}^{\infty} T_{e6n} \tag{7}$$

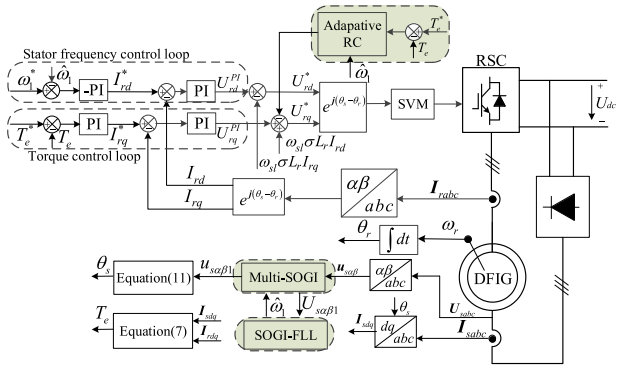

Fig. 3. RSC control scheme for torque and frequency regulation.

where $\hat{}$ represents the conjugate, T_{e0} represents the average torque, and T_{e6n} represents the torque ripple of 6*n*th-order fundamental frequency.

Combining (5), (6), and (7), the torque ripple can be expressed by the stator fundamental and harmonic currents as

$$\sum_{n=1}^{\infty} T_{e6n} = \sum_{n=1}^{\infty} \frac{2U_{\text{dc}}}{\pi} \text{Re} \begin{bmatrix} \left(\hat{\boldsymbol{I}}_{sdq(6n+1)} - \frac{\hat{\boldsymbol{I}}_{sdq1}}{(6n-1)^2} \right) e^{-j6n\omega_1 t} \\ + \left(\hat{\boldsymbol{I}}_{sdq(6n-1)} + \frac{\hat{\boldsymbol{I}}_{sdq1}}{(6n+1)^2} \right) e^{j6n\omega_1 t} \end{bmatrix}. \tag{8}$$

As seen from (8), the torque ripple contains many items, which consist of the stator fundamental current, positive harmonic currents, and negative harmonic currents. The torque ripple is abundant, which is harmful for the mechanical components of DFIG. Thus, an adaptive repetitive control method is applied to suppress the torque ripple, which will be elaborated in the Section III.

III. Adaptive Control Strategy of RSC

Since the dc voltage is constant, the DFIG is controlled to work in the MPPT mode. Thus, it is essential to propose a control strategy for the DFIG to track the torque reference accurately and suppress the torque ripple effectively. In order to track the torque reference accurately, orientation control is necessary for the decoupling control of the torque and flux. The stator fundamental voltage is obtained by the multi-SOGI block. The stator fundamental voltage is applied in the FLL block for acquiring the stator frequency, and the stator fundamental voltage vector is directly applied for acquiring the orientation angle. The torque ripple is suppressed by applying the adaptive RC directly into the current control loop.

The RSC control scheme for the torque control is shown in Fig. 3, which mainly consists of a multi-SOGI block, an FLL block, and an adaptive RC. The output of the adaptive RC is directly added to the *q*-axis rotor voltage reference to accurately suppress the torque ripple when the stator frequency changes. The multi-SOGI block, FLL block, and adaptive RC block will be elaborated in detail in the following three sections.

A. Angle of the Stator Fundamental Flux

It should be noted that the highly distorted stator voltage is not suitable for orientation. The stator flux is the integrator of stator voltage, which has little harmonics compared to the stator

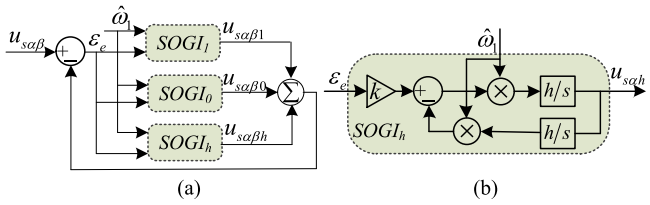

Fig. 4. Fundamental flux estimator based on multi-SOGI blocks. (a) Multi-SOGI blocks and (b) SOGI block with *h*th-order fundamental frequency.

voltage and is more appropriate for orientation. In [8] and [9], the stator flux vector is acquired by the integrator link or the inertial link for obtaining the orientation angle. However, the pure integrator is difficult to be applied practically because of the dc offset and initial value. If the inertial link is applied for acquiring the stator flux, the sampling dc offset also exists, which will cause the fundamental frequency pulsation in the angle and frequency. Furthermore, the magnitude and phase error at the fundamental frequency will deteriorate the decoupling control performance, which should be compensated additionally [18]. In this part, the stator fundamental voltage is acquired based on adaptive multi-SOGI block for orientation, which can avoid acquiring the stator flux.

As can be seen from Fig. 4(a), the SOGI_1 block is used to acquire the stator fundamental voltage, the SOGI_0 block is used to acquire the dc offset of stator voltage, and the SOGI_h block is used to acquire the harmonic components of stator voltage. As can be seen from the SOGI_h block in Fig. 4(b), the transfer function can be expressed as

$$G_{\text{SOGI}_h}(s) = \frac{kh\hat{\omega}_1 s}{s^2 + h^2\hat{\omega}_1^2}. \tag{9}$$

As can be seen from the expression of SOGI_h, each SOGI is a resonant controller and the resonant frequency is $h\hat{\omega}_1$, where $\hat{\omega}_1$ is the estimated stator frequency. It should be pointed out that the resonant controller turns to be an integrator when h is equal to zero.

Thus, the transfer function from the input stator voltage to the stator fundamental voltage can be expressed as

$$A(s) = \frac{u_{s\alpha 1}}{u_{s\alpha}} = \frac{G_{\text{SOGI}_1}(s)}{1 + \sum_{h=0,1,\ldots} G_{\text{SOGI}_h}(s)}. \tag{10}$$

Since the harmonics in stator voltage are mainly 5th-, 7th-, 11th-, 13th-, 17th-, and 19th-order fundamental frequency, the value of h in the multi-SOGI block are set as 0, 1, 5, 7, 11, 13, 17, and 19 correspondingly. Thus, the bode diagram of $A(s)$, pure integrator, and first-order low-pass filter can be plotted as shown in Fig. 5.

As can be seen from Fig. 5, the sampling dc offset is not restrained by the pure integrator or first-order low-pass filter. Furthermore, there exists 9° phase error in the first-order low-pass filter, which will deteriorate the decoupling control performance. However, unity magnitude response with zero phase shift for the fundamental frequency is achieved by the multi-SOGI block. Furthermore, the magnitude response for the dc and harmonic frequencies are all highly attenuated, which shows

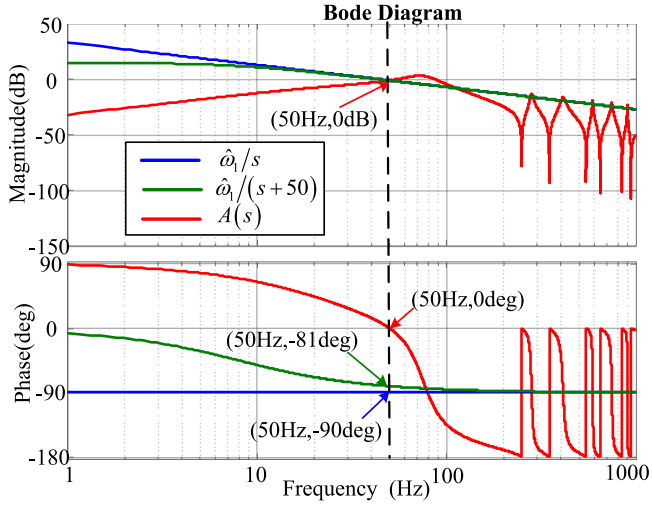

Fig. 5. Bode diagram of $A(s)$, pure integrator, and first-order low-pass filter.

a good filtering ability for the distorted stator voltage. Thus, the stator fundamental voltage and flux are obtained by the adaptive multi-SOGI block, which can avoid the pure integrator block and filter out the harmonics. Thus, the angle of the stator flux can be expressed as

$$\theta_s = \arctan\left(u_{s\beta 1}/u_{s\alpha 1}\right) - \frac{\pi}{2}. \tag{11}$$

The angle of stator flux is used as orientation angle, which can achieve the decoupling control of the stator frequency and torque.

B. Stator Frequency Estimation

There are several methods for estimating the stator frequency by PLL or FLL in the existed literature [10], [11], [17], [18]. Due to the highly distorted stator voltage, a low-pass filter is applied in PLL for reducing the stator frequency ripples [10], [11]. However, certain low-order harmonics, such as the 5th and 7th order, are very close to the fundamental frequency. Thus, these low-order harmonics lead to substantial ripples at the estimated stator frequency, which is not suitable for the adaptive repetitive control. In this part, the SOGI-FLL block is applied for estimating the stator frequency and the stator fundamental voltage is used as the input, which can avoid the harmonics and keep the better dynamic performance in just acquiring the stator frequency compared with the conventional PLL.

Fig. 6 shows the scheme diagram of the frequency estimation method based on an SOGI, which works as a phase discriminator. In Fig. 6, $\boldsymbol{U}_{s1}$ is the stator fundamental voltage vector, which is chosen as the input of the SOGI, while vector $\boldsymbol{V}_{s1}$ is defined as the output, and θ is the phase difference between $\boldsymbol{U}_{s1}$ and $\boldsymbol{V}_{s1}$. ω_1 is the actual stator frequency, and $\hat{\omega}_1$ represents the estimated frequency, which is also set as the resonant frequency of the SOGI. k_{ie} is the gain of the integrator and ω_{base} is the frequency base. Since the input voltage $\boldsymbol{U}_{s1}$ has been transformed to the unit form, the voltage amplitude compensation is not necessary and the loop gain is not sensitive to the voltage amplitude. In order to demonstrate the frequency estimation mechanism,

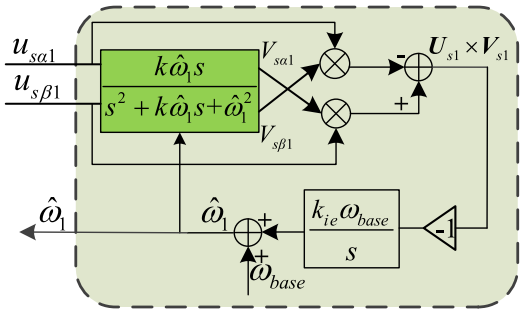

Fig. 6. Scheme diagram of the SOGI-FLL.

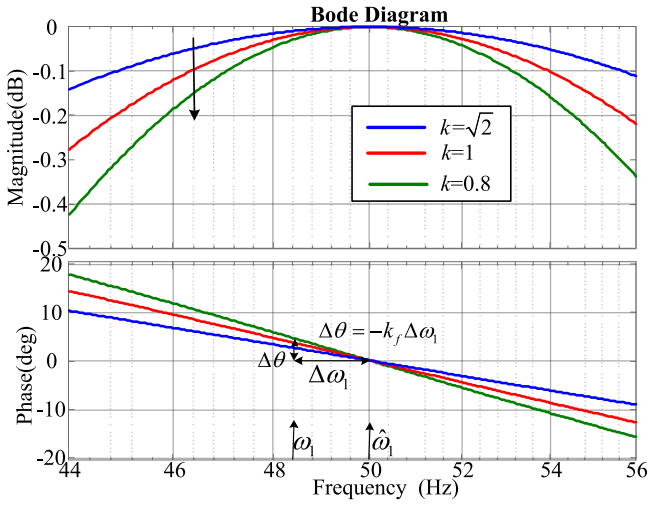

Fig. 7. Bode diagram of SOGI resonant at 50 Hz with different k.

Fig. 7 shows the bode diagram of the SOGI with the resonant frequency of $\hat{\omega}_1$.

It can be seen in Fig. 7 that θ is equal to 0^0 when $\omega_1 = \hat{\omega}_1$, which indicates that the cross product of vectors $\boldsymbol{U}_{s1}$ and $\boldsymbol{V}_{s1}$ is zero when the estimated frequency is equal to the actual stator frequency. When the estimated frequency deviates from the stator frequency, for example, if $\theta > 0^0$, it means $\omega_1 < \hat{\omega}_1$, and $\hat{\omega}_1$ should decrease correspondingly. Thus, the negative sign is added behind the cross product. Besides, at the adjacent of $\hat{\omega}_1$, the relation between the frequency estimation error $\Delta\omega_1$ and $\Delta\theta$ behave as linear correlation, which can be written as

$$\Delta\theta = -k_f \Delta\omega_1 \tag{12}$$

where k_f represents the linear factor, which is the inverse ratio with k. The detailed analysis and design of k_f will be demonstrated in the next section.

In this study, $\Delta\theta$ can be derived from the cross product between $\boldsymbol{U}_{s1}$ and $\boldsymbol{V}_{s1}$

$$\boldsymbol{U}_{s1} \times \boldsymbol{V}_{s1} = |\boldsymbol{U}_{s1}|\,|\boldsymbol{V}_{s1}| \sin(\Delta\theta) \approx |\boldsymbol{U}_{s1}|\,|\boldsymbol{V}_{s1}|\,\Delta\theta. \tag{13}$$

Once $\hat{\omega}_1$ converges to ω_1, $\boldsymbol{U}_{s1} \times V_{s1}$ will decrease to zero. For simplicity, $\boldsymbol{U}_{s1} \times V_{s1}$ can be directly chosen as the input error of the integrator, which is employed to remove the steady-state error. It should be pointed out that the PI regulator is substituted by the pure integrator for better filtering capability. ω_{base} is added as a frequency feedforward term for better dynamic response when the DFIG system starts.

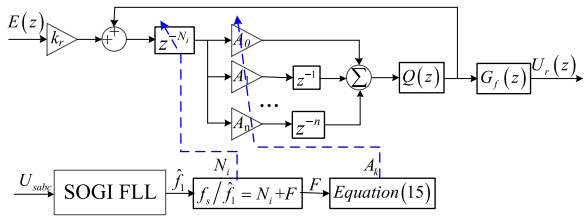

Fig. 8. Block diagram of the frequency-adaptive RC.

C. Adaptive RC

As mentioned earlier, the stator frequency is not imposed by the grid, which needs to be controlled additionally. Normally, the stator frequency is controlled to be the rated value when the output power is high. However, when the output power is low, the stator frequency can be controlled higher than the rated value to reduce the stator flux linkage for efficiency optimization [12]. In this way, the stator frequency variation over a wide range should be guaranteed. As can be seen from (8), the frequency of the torque ripple corresponds with the stator frequency. Thus, in order to suppress the torque ripple completely, a frequency-adaptive RC should be designed considering the stator frequency variation. The order N (the ratio of the sampling frequency to the stator frequency) would often be fractional with a mutative stator frequency and fixed sampling rate f_s. According to the fractional delay filters design method [21], the fractional delay (FD) $z^{-\mathrm{N}}$ can be well approximated by FD filters with integer orders. Assuming that $z^{-N} = z^{-N_i - F}$, with $N_i = \text{int}[N]$ being the integer part of N and $F = N - N_i\,(0 < F < 1)$ being the fractional part of N, the fractional delay $z^{-\mathrm{N}}$ can be approximated by a Lagrange interpolation polynomial FIR filter as

$$z^{-F} \approx \sum_{k=0}^{n} A_k z^{-k} \tag{14}$$

where $k = 0, 1, \ldots, n$, and the coefficient A_k can be obtained as

$$A_k = \prod_{\substack{i=0 \\ i \neq k}}^{n} \frac{F-i}{k-i}, \qquad k, i = 0, 1, \ldots, n. \tag{15}$$

The FD filters with different n have been investigated in [15]. Since the maximum considerable torque ripple frequency is less than 1000 Hz, thus $n = 2$ is enough for the accuracy of the FD filter in this paper. The transfer function of the adaptive RC used in this paper can be expressed as

$$G_{ARC}(z) = k_r \frac{z^{-N_i} \sum_{k=0}^{n} A_k z^{-k} Q(z)}{1 - z^{-N_i} \sum_{k=0}^{n} A_k z^{-k} Q(z)} G_f(z) \tag{16}$$

where k_r is the gain of the RC, Q(z) is a low-pass filter, and G_f(z) is a feed-forward phase compensator. The block diagram of frequency-adaptive RC is shown as Fig. 8. This RC provides a general approach for tracking or elimination of any periodic

signal with arbitrary fundamental frequency. Since the resonant frequency of RC corresponds with the stator frequency, there is no need to consider the bandwidth of RC anymore. Thus, $Q(z) = 0.2z + 0.8 + 0.1z^{-1}$, which is a low-pass filter to enhance the system robustness [21].

Finally, the rotor voltage reference can be expressed as

$$\boldsymbol{U}_{rdq}^{*} = \boldsymbol{U}_{rdq}^{PI} + \boldsymbol{U}_{rdq}^{RC} + j\sigma L_r \omega_{sl} \boldsymbol{I}_{rdq} \tag{17}$$

where $\boldsymbol{U}_{\text{rdq}}^{\text{PI}}$ is the output of the PI controller, $U_{\text{rdq}}^{\text{RC}}$ is the output of the adaptive RC, and $j\sigma\omega_{sl}L_r I_{rdq}$ is the cross-coupling terms as feed-forward item [13].

IV. Control Performance Analysis

In this section, based on the transfer function, the parameters of PI controllers and SOGI-FLL are designed for optimizing system performance. Furthermore, the control performance of torque ripple is also analyzed for validating the effectiveness of adaptive RC. Since the control of stator frequency and torque is decoupled, these two control loops can be analyzed separately. For the stator frequency control, the forward path is the *d*-axis rotor current control and the feedback is the SOGI-FLL for estimating the stator frequency. Thus, for analyzing the control performance of the stator frequency, the transfer function of the SOGI-FLL should be acquired first.

A. Parameter Design of the SOGI-FLL

The mathematical model of the proposed SOGI-FLL is derived in this section for the parameters design. To simplify the modeling process, the adaptive multi-SOGI block, which is applied for extracting the stator fundamental voltage is not considered.

For the SOGI block, the phase response of the SOGI can be expressed as

$$\theta_{\text{SOGI}}(\omega) = \begin{cases} 90^\circ - \arctan\left(\frac{k\hat{\omega}_1\omega}{\hat{\omega}_1^2-\omega^2}\right), & \omega < \hat{\omega}_1 \\ \arctan\left(\frac{k\hat{\omega}_1\omega}{\hat{\omega}_1^2-\omega^2}\right) - 90^\circ, & \omega > \hat{\omega}_1. \end{cases} \tag{18}$$

When the stator frequency is very equal to the resonant frequency $\hat{\omega}_1$, the relationship between the frequency and the phase angle can be expressed as

$$\frac{\Delta\theta}{\Delta\omega} = \lim_{\omega\to\hat{\omega}_1} \frac{-k\hat{\omega}_1\left(\omega^2+\hat{\omega}_1^2\right)}{\left(\omega^2-\hat{\omega}_1^2\right)^2 + \left(k\hat{\omega}_1\omega\right)^2} = \frac{-2}{k\hat{\omega}_1}. \tag{19}$$

When the stator voltage is expressed in per unit, the cross product of $\boldsymbol{U}$ and $\boldsymbol{V}$ in (13) can be expressed as

$$\boldsymbol{U} \times \boldsymbol{V} = -\frac{2}{k\hat{\omega}_1}\Delta\omega = -k_f\Delta\omega. \tag{20}$$

As can be seen from (20), k_f is the inverse ratio with k, which corresponds with Fig. 7. Combining (13), (19), and (20), the block diagram of SOGI-FLL can be expressed as shown in Fig. 9.

Thus, the transfer function of the SOGI-FLL can be expressed as

$$G_{\text{FLL}}(s) = \frac{k_f k_{ie}\omega_{\text{base}}}{s + k_f k_{ie}\omega_{\text{base}}}. \tag{21}$$

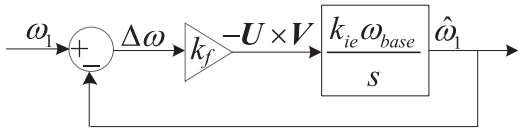

Fig. 9. Block diagram of SOGI-FLL.

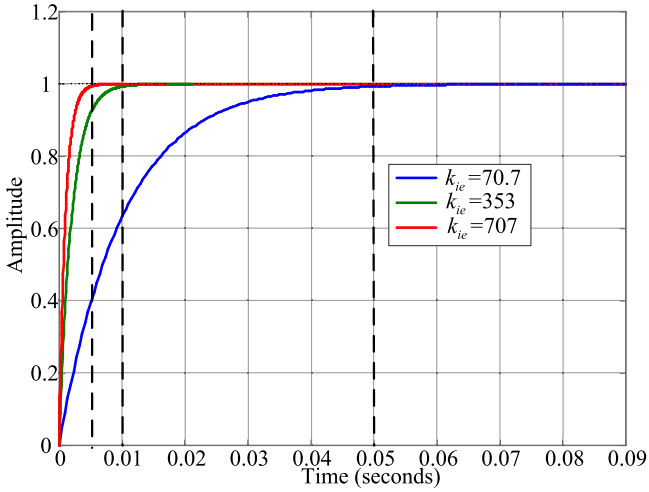

Fig. 10. Step response of SOGI-FLL.

Thus, the dynamic performance of the SOGI-FLL block depends on the SOGI parameter k and the integrator coefficient k_{ie}. The SOGI parameter k is always set as 1.414 for the quick dynamic performance of SOGI [18]. With a high value of the integrator coefficient k_{ie}, the stator frequency can be obtained quickly. The transfer function of the SOGI-FLL block is a first-order inertia block, which is simpler than the conventional PLL with low-pass filter and easier for parameter design. The step response of the SOGI-FLL with different k_{ie} is shown in Fig. 10. As can be seen from Fig. 10, with higher k_{ie}, higher bandwidth of the SOGI-FLL block can be acquired. When k_{ie} is equal to 707, the stator frequency can be acquired in 5 ms. Since the input voltage of SOGI-FLL is in per unit, k_{ie} is also in per unit. All the controlled variables and parameters are all in per unit in this paper. However, if the bandwidth of the FLL block is too high, it may cause the system instability or oscillation [18]. Thus, for ensuring the system stability and frequency response of SOGI-FLL in millisecond level, the integrator coefficient k_{ie} is valued as 707.

B. Performance of Frequency Control Loop

Since the stator current is active current, the exciting current is completely supplied by the *d*-axis rotor current. Thus, the stator flux linkage can be expressed as

$$\boldsymbol{\psi}_s = L_m \boldsymbol{I}_{rd}. \tag{22}$$

The stator frequency can be expressed as

$$\omega_1 = \frac{e_{sq}}{\psi_s} = \frac{u_{sq} - r_s I_{rq}}{\psi_s}. \tag{23}$$

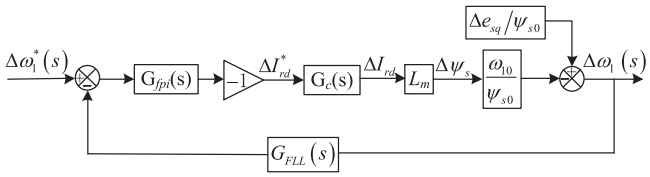

Fig. 11. Block diagram of the frequency control loop.

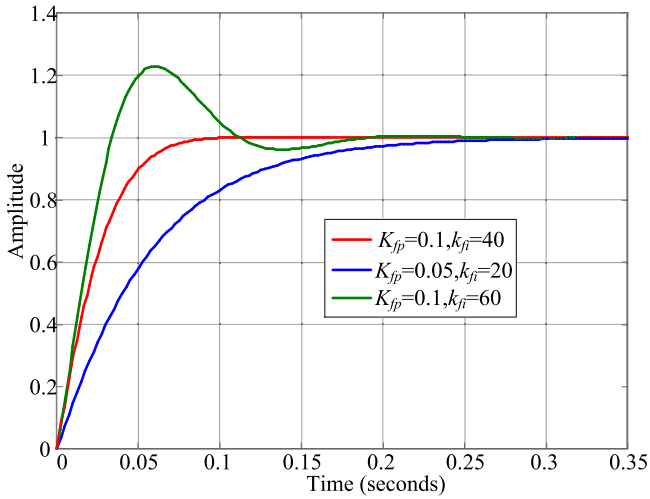

Fig. 12. Step response of the stator frequency.

The relationship between the stator frequency and the stator flux linkage is nonlinear. Assuming that the steady operating point is $\omega_{10} = (u_{sq0} - r_s I_{rq0})/\psi_{s0}$, the linear small signal model can be obtained as

$$\Delta\omega_1 = \frac{\Delta e_{sq}}{\psi_{s0}} - \frac{\omega_{10}}{\psi_{s0}}\Delta\psi_s \tag{24}$$

where

$$\Delta e_{sq} = \Delta u_{sq} - r_s \Delta I_{rq}. \tag{25}$$

Combining (21) and (22)–(25), the simplified frequency control loop can be expressed as shown in Fig. 11, where $G_{fpi}(s)$ represents the outer frequency PI controller and the inner current control loop is equivalent to a first-order system $G_c(s)$ for simplicity.

According to Fig. 11, the open-loop transfer function of a stator frequency can be expressed as

$$G_{\text{open}}(s) = \frac{L_m \omega_{10}}{\psi_{s0}} G_{fpi}(s)\, G_c(s)\, G_{\text{FLL}}(s). \tag{26}$$

In order to get a quick and steady stator frequency response, the closed-loop transfer function is always designed to be a first-order system. Since the sampling frequency is 10 kHz in this paper, the bandwidth of the inner loop is designed as 400 rad/s. Thus, the stator frequency response with different PI parameters of $G_{fpi}(s)$ is shown in Fig. 12. As can be seen from Fig. 12, if the bandwidth of the outer loop is high, there exists a frequency overshoot. Thus, the bandwidth of the stator frequency loop is designed as 40 rad/s. For reducing the system order, the PI parameters of $G_{fpi}(s)$ should correspond with the inner control loop according to the zero–pole cancellation theory. The proportional parameter and the integrator coefficient of $G_{fpi}(s)$ are 0.1 and 40, which are both in per unit.

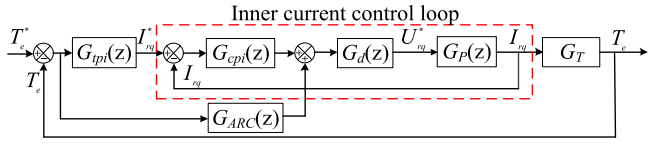

Fig. 13. Block diagram of the torque control loop.

C. Performance of Torque Control Loop

According to the RSC control scheme in Fig. 3, the block diagram of torque control loop can be expressed as shown in Fig. 13. Although the performance of RC in suppressing torque ripple has been demonstrated in [15], the torque outer loop is ignored in [15] and is considered in this paper. In order to validate the effectiveness of torque ripple suppression ability of RC just added in the q-axis, the relationship between the torque ripple and the harmonic currents is deduced. For the simplicity of the torque ripple expression, only the torque ripple of the sixth-order frequency harmonic is considered.

The stator flux containing harmonics in the synchronous dq frame can be expressed as

$$\boldsymbol{\psi}_{sdq} = (\psi_{sd1} + \psi_{sd6}) + j\,(\psi_{sq1} + \psi_{sq6}) \tag{27}$$

where ψ_{sd1} and ψ_{sq1} are the fundamental components, which are dc quantities, and ψ_{sd6} and ψ_{sq6} are the harmonic components, which are ac components with the sixth-order fundamental frequency.

The rotor current containing harmonics in the synchronous dq frame can be expressed as

$$\boldsymbol{I}_{rdq} = (I_{rd1} + I_{rd6}) + j\,(I_{rq1} + I_{rq6}) \tag{28}$$

where I_{rd1} and I_{rq1} are the fundamental components, which are dc quantities, and, I_{rd6} and I_{rq6} are the harmonic components, which are ac components with the sixth-order fundamental frequency.

In this way, the torque can be expressed as

$$T_e = -\frac{L_m}{L_s}\left((\psi_{sd1} I_{rq1}) + (\psi_{sd1} I_{rq6} + \psi_{sd6} I_{rq1} - \psi_{sq6} I_{rd1}) + (\psi_{sd6} I_{rq6} - \psi_{sq6} I_{rq6})\right). \tag{29}$$

As can be seen from the torque expression, the second term in (29) is the sixth-order harmonic components. Thus, the torque ripple of the sixth-order fundamental frequency can be expressed as

$$T_{e6} = -\frac{L_m}{L_s}(\psi_{sd1} I_{rq6}) - \frac{L_m}{L_s}(\psi_{sd6} I_{rq1} - \psi_{sq6} I_{rd1}). \tag{30}$$

As can be seen from the expression, the second term in (30) consists of the stator harmonic flux and the rotor fundamental current, which are constant if the stator voltage and working point are fixed. In this way, the second term can be seen as a disturbance term. Thus, the torque ripple can be controlled to zero just by regulating the q-axis rotor harmonic current.

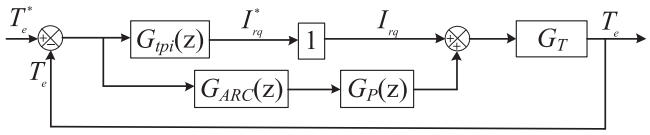

Fig. 14. Block diagram of the simplified torque control loop.

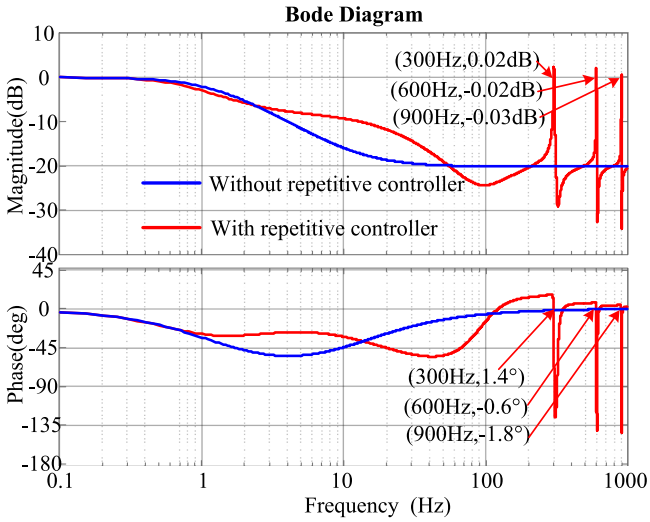

Fig. 15. Bode diagram of the torque control loop.

Therefore, the torque ripple can be eliminated completely even just by adding an RC on the torque loop (q-axis).

Since adaptive RC is expressed in the discrete Z domain, the torque and current PI controllers are both expressed in the Z domain. Where $G_{tpi}(z)$ represents the torque PI controller, $G_{cpi}(z)$ represents the current PI controller, and $G_p(z)$ represents the transfer function of DFIG $G_T = \psi_{s0} \cdot L_m / L_s$.

Since the bandwidth of the inner current control loop is higher than the outer torque loop, the inner current loop can be seemed as unit block and the simplified torque control loop can be expressed as shown in Fig. 14.

According to Fig. 14, the transfer function from the torque reference to the output torque can be expressed as

$$G_{T_e}(z) = \frac{T_e}{T_e^*} = \frac{\left(G_{tpi}(z) + G_{ARC}(z)G_P(z)\right) G_T}{1 + \left(G_{tpi}(z) + G_{ARC}(z)G_P(z)\right) G_T}. \tag{31}$$

The bode diagram of the transfer function (31) with and without adaptive RC is shown in Fig. 15.

As can be shown in Fig. 15, when the adaptive RC is not added, the torque control loop has no control ability at the harmonic frequencies. However, the response of the harmonic frequencies are all unit responses when the adaptive RC is added, which indicate the ability of suppressing torque ripple. The detailed parameter design of RC has been demonstrated in [15], which is not repeated in this paper.

V. Experimental Results

In order to validate the control strategy proposed in Section III, a DFIG-DC experimental system is developed.

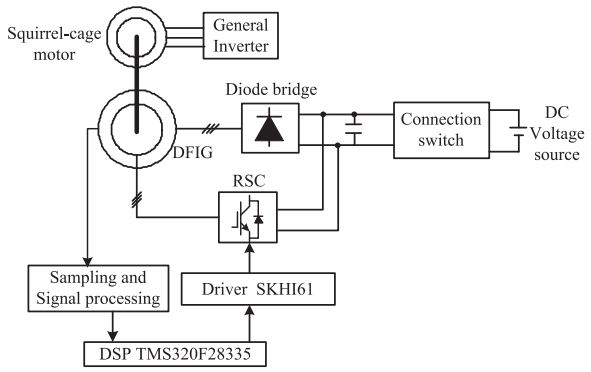

Fig. 16. Schematic diagram of the experiment system.

Fig. 17. Experimental setup of the DFIG-DC system.

TABLE I
Parameters of DFIG

Parameters	*Value*	*Parameters*	*Value*
Rated power	1.0 kW	Rated voltage	110 V
Rated frequency	50 Hz	DC voltage	140 V
Stator/rotor	0.33	R_s	1.01 Ω
R_r	0.88 Ω	L_m	87.5 mH
$L_{\sigma s}$	5.6 mH	$L_{\sigma r}$	5.6 mH

The schematic diagram of the experimental system is shown in Fig. 16. The photograph of experimental setup is shown in Fig. 17. The DFIG was driven by a squirrel-cage induction motor with the control of a general inverter. The control strategy of RSC is implemented on the TI TMS320F28335 DSP, and the switching frequency is 10 kHz with a sampling frequency of 10 kHz. The parameters of the DFIG are shown in Table I. The pole pairs of DFIG is 3, and the synchronous speed is 1000 r/min when the stator frequency is controlled to be 50 Hz. All the waveforms are acquired by a YOKOGAWA DL750 scope.

Fig. 18 shows the comparison results of three stator frequency estimation methods on the condition of the stator frequency variation from 50 to 55 Hz, in which ω_{sFLL} represents the stator

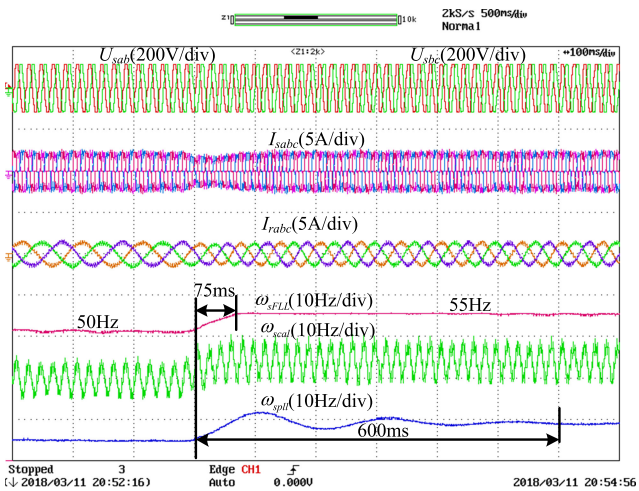

Fig. 18. Comparison results of the three frequency estimation methods.

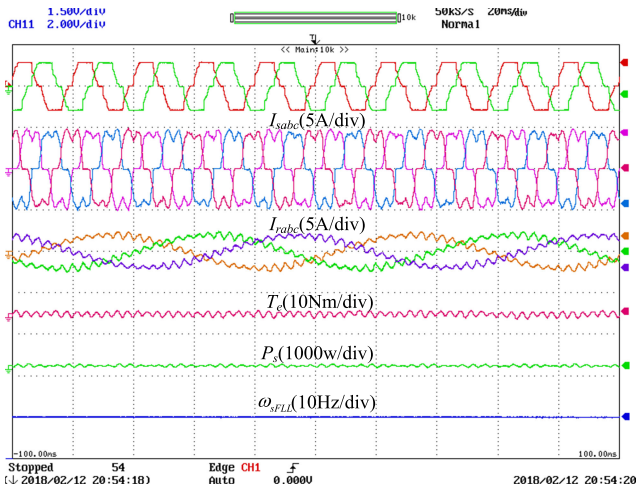

Fig. 19. Experimental results of DFIG with adaptive RC disabled.

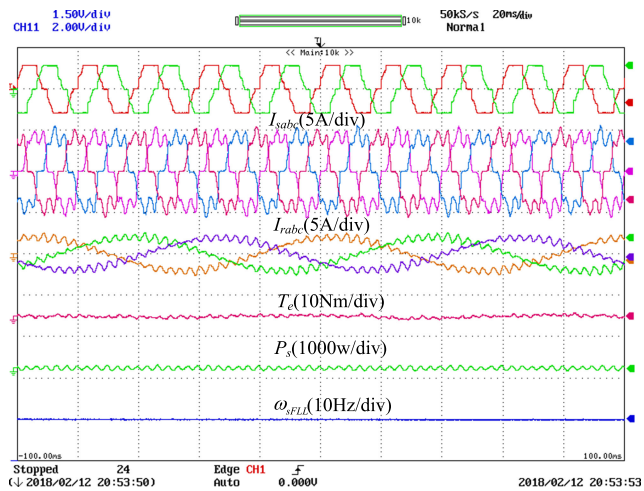

Fig. 20. Experimental results of DFIG with adaptive RC enabled.

frequency obtained from the SOGI-FLL block, ω_{scal} represents the stator frequency obtained from the derivative of the stator flux linkage angle [14], and ω_{spll} represents the stator frequency obtained from the low-bandwidth PLL block [11]. As can be seen from Fig. 18, ω_{scal} not only contains the sixth-order harmonics but also contains 50 Hz harmonics, which is caused by the dc offset in the sampled stator voltage. ω_{spll} contains no harmonics while has a slow dynamic response within 600 ms when the stator frequency varies. However, ω_{sFLL} not only contains no harmonic but also has a good dynamic response within 75 ms, which is necessary for the adaptive repetitive control.

Fig. 19 shows the steady-state experimental results of the DFIG system when the adaptive RC is disabled. In the experimental tests, the torque reference is -7.64 N·m (-0.8 pu) and the stator power transferred to the dc voltage source is 800 W. The rotor speed is 800 r/min and the stator frequency is regulated to 50 Hz. As can be seen from the torque waveform, the maximum torque ripple is 0.55 N·m (7.2%). It is necessary to employ the adaptive RC to suppress the torque ripple.

Fig. 20 shows the steady-state experimental results of the DFIG system when the adaptive RC is enabled, in which the operation condition is the same as Fig. 19. It can be seen that the torque ripple reduces to 0.05 N·m (0.6%), which is greatly suppressed. Thus, the adaptive RC shows the satisfied performance in reducing the torque ripple. Furthermore, the stator frequency estimation is not influenced by the adaptive RC. The stator harmonic current contents with and without the adaptive RC are shown in Table II. As can be seen from Table II, when suppressing the torque ripple, the $(6n-1)$th-order harmonic current is decreased and the $(6n+1)$th$-$order harmonic is increased; thus, the total harmonic distortion (THD) of the stator current is not increased. In this way, the reduction of torque ripple has no influence on the power loss of system.

Fig. 21 shows the dynamic experimental results of the DFIG system when the stator frequency varies from 50 to 60 Hz with the adaptive RC enabled. As can be seen from Fig. 21, the torque ripple becomes larger when the stator frequency varies due to the slow dynamic response of the RC. When the stator frequency reaches to 60 Hz in steady state, the adaptive RC is effective in suppressing the torque ripple, which validates the proposed adaptive strategy.

Fig. 22 shows the experimental results of the DFIG system with adaptive RC enabled when the rotor speed varies from 800 to 1200 r/min. In the experimental tests, the torque reference is -4.78 N·m (-0.5 pu) and the stator power transferred to the dc voltage source is 500 W. The stator frequency is regulated to 50 Hz. The rotor power waveform is added in this figure, and the reference direction of the rotor power is from the dc link to the rotor inverter. Thus, when the rotor speed changes from 800 to 1200 r/min, the rotor powers changes form positive to negative. As can be seen from the torque waveform, the torque ripple is always 0.04 N·m (0.8%), which is not affected by the changes of the rotor speed. Therefore, the proposed control strategy can well suppress the torque ripple for both the subsynchronous and supersynchronous operation mode.

TABLE II
STATOR HARMONIC CURRENT CONTENTS WITH OR WITHOUT ADAPTIVE RC

Harmonic order	5^{th}	7^{th}	11^{th}	13^{th}	17^{th}	19^{th}	THD
Without RC	20.45%	6.10%	4.30%	1.78%	1.86%	0.42%	24.34%
With RC	13.44%	17.94%	2.09%	2.31%	1.10%	1.26%	24.94%

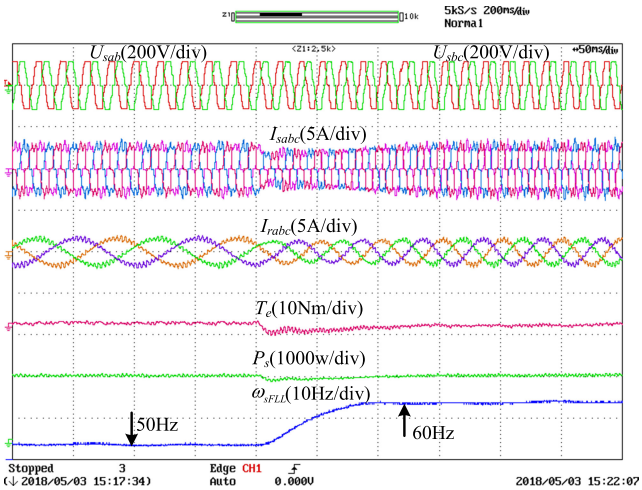

Fig. 21. Experimental results of DFIG with stator frequency variation.

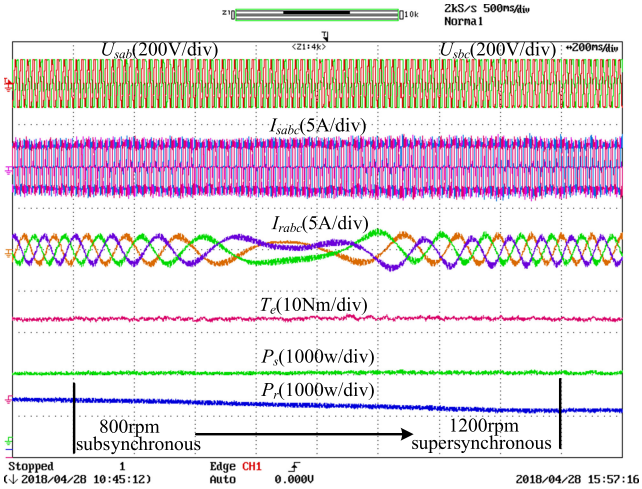

Fig. 22. Experimental results of DFIG with rotor speed varying from 800 to 1200 r/min.

VI. CONCLUSION

The adaptive repetitive control of DFIF-DC system for torque ripple suppression is proposed in this paper considering the system efficiency optimization. Grounded on the proposed method, three main contributions can be achieved as follows.

1) The multi-SOGI block is applied for acquiring the stator fundamental voltage, which can eliminate the effect of dc offset and harmonics in the stator voltage. Furthermore, the SOGI-FLL block is proposed for acquiring the stator frequency to avoid the fundamental frequency and harmonic frequency ripples.
2) The stator fundamental voltage vector is directly applied for acquiring the orientation angle, which can reduce the parameter dependency on the stator and rotor inductance.
3) The adaptive RC is used for suppressing the torque ripple considering the stator frequency variation for improving system efficiency.

REFERENCES

[1] R. Cardenas, R. Pena, S. Alepuz, and G. Asher, "Overview of control systems for the operation of DFIGs in wind energy applications," *IEEE Trans. Ind. Electron.*, vol. 60, no. 7, pp. 2776–2798, Jul. 2013.
[2] F. Blaabjerg, M. Liserre, and K. Ma, "Power electronics converters for wind turbine systems," *IEEE Trans. Ind. Appl.*, vol. 48, no. 2, pp. 708–719, Mar.–Apr. 2012.
[3] C. Du, E. Agneholm, and G. Olsson, "Comparison of different frequency controllers for a VSC-HVDC supplied system," *IEEE Trans. Power. Del.*, vol. 23, no. 4, pp. 2224–2232, Oct. 2008.
[4] E. M. D. Miguel, S. M. David, A. Santiago, and D. C. Edgardo, "Optimal operation of offshore wind farms with line-commutated HVDC link connection," *IEEE Trans. Energy Convers.*, vol. 25, no. 2, pp. 71–78, Jun. 2010.
[5] B. G. Ramon *et al.*, "Diode-based HVDC link for the connection of large offshore wind farms," *IEEE Trans. Energy Convers*, vol. 26, no. 2, pp. 615–626, Jun. 2011.
[6] X. Yao, H. Sui, and Z. Xing, "The study of VSC-HVDC transmission system for offshore wind power farm," in *Proc. Int. Conf. Elect. Mach.*, 2007, pp. 314–319.
[7] M. F. Iacchetti, G. D. Marques, and R. Perini, "Operation and design issues of a DFIG stator-connected to a DC-net by a diode rectifier," *IET Elect. Power Appl.*, vol. 8, no. 8, pp. 310–319, Sep. 2014.
[8] G. D. Marques and M. F. Iacchetti, "Stator frequency regulation in a field oriented controlled DFIG connected to a DC link," *IEEE Trans. Ind. Electron.*, vol. 61, no. 11, pp. 5930–5939, Nov. 2014.
[9] G. D. Marques and M. F. Iacchetti, "Inner control method and frequency regulation of a DFIG connected to a DC link," *IEEE Trans. Energy Convers.*, vol. 29, no. 2, pp. 435–444, Jun. 2014.
[10] G. D. Marques and M. F. Iacchetti, "Air-gap power-based sensorless control in a DFIG connected to a DC link," *IEEE Trans. Energy Convers.*, vol. 30, no. 1, pp. 367–375, Mar. 2015.
[11] G. D. Marques and M. F. Iacchetti, "A self-sensing stator-current-based control system of a DFIG connected to a DC-link," *IEEE Trans. Ind. Electron.*, vol. 62, no. 10, pp. 6140–6150, Oct. 2015.
[12] G. D. Marques and M. F. Iacchetti, "Field-weakening control for efficiency optimization in a DFIG connected to a DC-link," *IEEE Trans. Ind. Electron.*, vol. 63, no. 6, pp. 3409–3419, Jun. 2016.
[13] M. F. Iacchetti, G. D. Marques, and R. Perini, "Torque ripple reduction in a DFIG-DC system by resonant current controllers," *IEEE Trans. Power Electron.*, vol. 30, no. 8, pp. 4244–4254, Aug. 2015.
[14] H. Nian, C. Wu, and P. Cheng, "Direct resonant control strategy for torque ripple mitigation of DFIG connected to DC link through diode rectifier on Stator," *IEEE Trans. Power Electron.*, vol. 32, no. 9, pp. 6936–6945, Sep. 2017.
[15] C. Wu and H. Nian, "An improved repetitive control of DFIG-DC system for torque ripple suppression," *IEEE Trans. Power Electron.*, vol. 33, no. 9, pp. 7634–7644, Sep. 2018.
[16] G. D. Marques and M. F. Iacchetti, "Minimization of torque ripple in the DFIG-DC system via predictive delay compensation," *IEEE Trans. Ind. Electron.*, vol. 65, no. 1, pp. 103–113, Jan. 2018.

[17] S. M. A. Cruz *et al.*, "Predictive torque and rotor flux control of a DFIG-DC system for torque-ripple compensation and loss minimization," *IEEE Trans. Ind. Electron.*, doi: 10.1109/TIE.2018.2818667.
[18] P. Rodriguez, A. Luna, I. Candela, R. Mujal, R. Teodorescu, and F. Blaabjerg, "Multiresonant frequency-locked loop for grid synchronization of power converters under distorted grid conditions," *IEEE Trans. Ind. Electron.*, vol. 58, no. 1, pp. 127–138, Jan. 2011.
[19] R. Zhao, Z. Xin, P. Loh, and F. Blaabjerg, "A novel flux estimator based on multiple second-order generalized integrators and frequency-locked loop for induction motor drives," *IEEE Trans. Power Electron.*, vol. 32, no. 8, pp. 6286–6296, Aug. 2017.
[20] D. Chen, J. Zhang, and Z. Qian, "An improved repetitive control scheme for grid-connected inverter with frequency-adaptive capability," *IEEE Trans. Ind. Electron.*, vol. 60, no. 2, pp. 814–823, Feb. 2013.
[21] D. Chen, J. Zhang, and Z. Qian, "An improved repetitive control scheme for grid-connected inverter with frequency-adaptive capability," *IEEE Trans. Ind. Electron.*, vol. 60, no. 2, pp. 814–823, Feb. 2013.
[22] Z. Zou, K. Zhou, Z. Wang, and M. Cheng, "Frequency-adaptive fractional-order repetitive control of shunt active power filters," *IEEE Trans. Ind. Electron.*, vol. 62, no. 3, pp. 1659–1667, Mar. 2015.

Chao Wu was born in Huanggang, China, in 1992. He received the B.Eng. degree in electrical engineering from the HeFei University of Technology, Hefei, China. He is currently working toward the Ph.D. degree in electrical engineering from Zhejiang University, Hangzhou, China.

His current research interests include the control strategy of doubly fed induction generators for dc power transmission in wind energy conversion systems.

Heng Nian (M'09–SM'14) received the B.Eng. degree and the M.Eng. degree from the HeFei University of Technology, Hefei, China, in 1999 and 2002, respectively, and the Ph.D. degree from Zhejiang University, Hangzhou, China, in 2005, all in electrical engineering.

From 2005 to 2007, he was as a Postdoctoral Research Fellow with the College of Electrical Engineering, Zhejiang University. In 2007, he was promoted as an Associate Professor. Since 2016, he has been a Full Professor at the College of Electrical Engineering, Zhejiang University. From 2013 to 2014, he was a Visiting Scholar in the Department of Electrical, Computer, and System Engineering, Rensselaer Polytechnic Institute, Troy, NY, USA. His current research interests include the optimal design and operation control for wind power generation system. He has authored or coauthored more than 20 IEEE/IET Transaction papers and holds more than 20 issued/pending patents.

Bo Pang was born in Anhui, China, in 1994. He received the B.Eng. degree in electrical engineering in 2016 from Zhejiang University, Hangzhou, China, where he is currently working toward the Ph.D.degree in electrical engineering.

His current research interests include the control strategy of doubly fed induction generators under nonideal grids in wind energy generation systems.

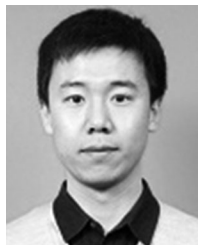

Peng Cheng received the B.Eng. and Ph.D degrees from the College of Electrical Engineering, Zhejiang University, Hangzhou, China, in July 2011 and June 2016, respectively, all in electrical engineering.

He is now an Engineer in the Renewable Energy Department, China Electric Power Research Institute (CEPRI), Beijing, China. His current research interests include the control and operation of the power electronics devices in the renewable-energy conversion. He has contributed in the reviewing process for several IEEE transactions and IET journals.